



1 **Ozone and haze pollution weakens net primary productivity in China**

2

3 Xu Yue¹, Nadine Unger², Kandice Harper³, Xiangao Xia⁴, Hong Liao⁵, Tong Zhu⁶,
4 Jingfeng Xiao⁷, Zhaozhong Feng⁸, and Jing Li⁹

5

6 ¹ Climate Change Research Center, Institute of Atmospheric Physics, Chinese Academy
7 of Sciences, Beijing 100029, China

8 ² College of Engineering, Mathematics and Physical Sciences, University of Exeter,
9 Exeter, EX4 4QE, UK

10 ³ School of Forestry and Environmental Studies, Yale University, 195 Prospect Street,
11 New Haven, Connecticut 06511, USA

12 ⁴ Laboratory for Middle Atmosphere and Global Environment Observation, Institute of
13 Atmospheric Physics, Chinese Academy of Sciences, Beijing 100029, China

14 ⁵ School of Environmental Science and Engineering, Nanjing University of Information
15 Science & Technology, Nanjing 210044, China

16 ⁶ State Key Laboratory for Environmental Simulation and Pollution Control, College of
17 Environmental Sciences and Engineering, Peking University, Beijing 100871, China.

18 ⁷ Earth Systems Research Center, Institute for the Study of Earth, Oceans, and Space,
19 University of New Hampshire, Durham, NH 03824, USA

20 ⁸ Research Center for Eco-Environmental Sciences, Chinese Academy of Sciences,
21 Beijing 100085, China

22 ⁹ Laboratory for Climate and Ocean-Atmosphere Studies, Department of Atmospheric
23 and Oceanic Sciences, School of Physics, Peking University, Beijing 100871, China

24

25

26 *Corresponding author:*

27 Xu Yue

28 Telephone: 86-10-82995369

29 Email: yuexu@mail.iap.ac.cn

30

31

32 *Keywords:* Haze pollution, climate projection, pollution mitigation, ozone damage,
33 diffuse radiative fertilization, aerosol radiative effects, aerosol indirect effects,
34 photosynthesis, net primary productivity

35



36

Abstract

37

38 Atmospheric pollutants have both beneficial and detrimental effects on carbon uptake by
39 land ecosystems. Surface ozone damages leaf photosynthesis by oxidizing plant cells,
40 while aerosols promote carbon uptake by increasing diffuse radiation and exert additional
41 influences through concomitant perturbations to meteorology and hydrology. China is
42 currently the world's largest emitter of both carbon dioxide and short-lived air pollutants.
43 The land ecosystems of China are estimated to provide a carbon sink, but it remains
44 unclear whether air pollution acts to inhibit or promote carbon uptake. Here, we employ
45 Earth system modeling and multiple measurement datasets to assess the separate and
46 combined effects of anthropogenic ozone and aerosol pollution on net primary
47 productivity (NPP) in China. In the present day, air pollution reduces annual NPP by 0.4
48 Pg C (9%), resulting from a decrease of 0.6 Pg C (14%) by ozone damage, and an
49 increase of 0.2 Pg C (5%) by aerosol direct effects. The enhancement by aerosols is a
50 combination of diffuse radiation fertilization, reduced canopy temperatures, and reduced
51 evaporation leading to higher soil moisture. However, precipitation inhibition from
52 combined aerosol direct and indirect effects reduces annual NPP by 0.2 Pg C (4%),
53 leading to a net air pollution suppression of 0.8 Pg C (16%). Our results reveal strong
54 dampening effects of air pollution on the land carbon uptake in China today. Following
55 the current legislation emission scenario, this suppression will not alleviate by the year
56 2030, mainly due to a continuing increase in surface ozone. However, the maximum
57 technically feasible reduction scenario could drastically relieve the current level of NPP
58 damage by 70% in 2030, offering protection of this critical ecosystem service and the
59 mitigation of long-term global warming.

60

61



62 1 Introduction

63

64 Surface ozone (O_3) and atmospheric aerosols influence land ecosystem carbon uptake
65 both directly and indirectly through Earth system interactions. O_3 reduces plant
66 photosynthesis directly through stomatal uptake. The level of damage is dependent on
67 both surface ozone concentrations ($[O_3]$) and the stomatal conductance (g_s), the latter of
68 which is closely related to the photosynthetic rate (Reich and Amundson, 1985; Sitch et
69 al., 2007; Ainsworth et al., 2012). The impact of aerosol pollution on vegetation is less
70 clear. Atmospheric aerosols influence plant photosynthesis through perturbations to
71 radiation, meteorology, and cloud. Observations (Cirino et al., 2014; Strada et al., 2015)
72 suggest that an increase in diffuse light partitioning in response to a moderate aerosol
73 loading can improve canopy light use efficiency (LUE) and promote photosynthesis,
74 known as diffuse radiation fertilization (DRF), as long as the total light availability is not
75 compromised (Kanniah et al., 2012). Atmospheric aerosols also reduce leaf temperature
76 (Steiner and Chameides, 2005; Cirino et al., 2014), but the consequence for
77 photosynthesis depends on the relationship between the local environmental temperature
78 and the photosynthetic optimum temperature of approximately 25°C . Aerosol-induced
79 changes in evaporation and precipitation are interconnected but impose opposite effects
80 on photosynthesis; less evaporation preserves soil moisture in the short term but may
81 decrease local rainfall (Spracklen et al., 2012) and lead to drought conditions in the long
82 term. Furthermore, aerosol indirect effects (AIE) on cloud properties can either
83 exacerbate or alleviate the above feedbacks.

84

85 China is currently the world's largest emitter of both carbon dioxide and short-lived air
86 pollutants (<http://gains.iiasa.ac.at/models/>). The land ecosystems of China are estimated
87 to provide a carbon sink (Piao et al., 2009), but it remains unclear how air pollution may
88 affect this sink through the atmospheric influences on regional carbon uptake. O_3
89 damages to photosynthesis, including those in China, have been quantified in hundreds of
90 measurements (Table S1), but are limited to individual plant species and specific $[O_3]$.
91 Previous regional modeling of O_3 vegetation damage (e.g., Ren et al., 2011; Tian et al.,
92 2011) does not always take advantage of valuable observations and typically the derived



93 results have not been properly validated. The aerosol effects on photosynthesis are less
94 understood. Most of the limited observation-based studies (Rocha et al., 2004; Cirino et
95 al., 2014; Strada et al., 2015) rely on long-term flux measurements or satellite retrievals,
96 which are unable to unravel impacts of changes in the associated meteorological and
97 hydrological forcings. Modeling studies focus mainly on the aerosol-induced
98 enhancement in diffuse radiation (e.g., Cohan et al., 2002; Gu et al., 2003; Mercado et al.,
99 2009), but ignore other direct and indirect feedbacks such as changes in temperature and
100 precipitation. Finally, no studies have investigated the combined effects of O₃ and
101 aerosols or how the air pollution influences may vary in response to future emission
102 regulations and climate change.

103

104 In this study, we assess the impacts of O₃ and aerosols on land carbon uptake in China
105 using the global Earth system model NASA GISS ModelE2 that embeds the Yale
106 Interactive Terrestrial Biosphere model (YIBs). This framework is known as NASA
107 ModelE2-YIBs and fully couples the land carbon-oxidant-aerosol-climate system
108 (Schmidt et al., 2014; Yue and Unger, 2015). The global-scale model accounts for long-
109 range transport of pollution and large-scale feedbacks in physical climate change. The
110 coupled Earth system simulations apply present-day and future pollution emission
111 inventories from the Greenhouse Gas and Air Pollution Interactions and Synergies
112 (GAINS) integrated assessment model (<http://gains.iiasa.ac.at/models/>). The simulations
113 include process-based, mechanistic photosynthetic responses to physical climate change,
114 O₃ stomatal uptake, carbon dioxide (CO₂) fertilization, and aerosol radiative
115 perturbations, but not aerosol and acid deposition (Table 1). The O₃ and aerosol haze
116 effects on the land carbon cycle fluxes occur predominantly through changes to gross
117 primary productivity (GPP) and net primary productivity (NPP). Therefore, the current
118 study focuses on GPP and NPP impacts and does not address changes in net ecosystem
119 exchange (NEE).

120

121 **2 Methods**

122

123 **2.1 YIBs vegetation model**



124

125 The YIBs model applies the well-established Farquhar and Ball-Berry models (Farquhar
126 et al., 1980; Ball et al., 1987) to calculate leaf photosynthesis and stomatal conductance,
127 and adopts a canopy radiation scheme (Spitters, 1986) to separate diffuse and direct light
128 for sunlit and shaded leaves. The assimilated carbon is dynamically allocated and stored
129 to support leaf development (changes in leaf area index, LAI) and tree growth (changes
130 in height). A process-based soil respiration scheme that considers carbon flows among 12
131 biogeochemical pools is included to simulate carbon exchange for the whole ecosystem
132 (Yue and Unger, 2015). Similar to many terrestrial models (Schaefer et al., 2012), the
133 current version of YIBs does not include a dynamic N cycle. Except for this deficit, the
134 vegetation model can reasonably simulate ecosystem responses to changes in [CO₂],
135 meteorology, phenology, and land cover (Yue et al., 2015). A semi-mechanistic O₃
136 vegetation damage scheme (Sitch et al., 2007) is implemented to quantify responses of
137 photosynthesis and stomatal conductance to O₃ (Yue and Unger, 2014).

138

139 The YIBs model can be used in three different configurations: site-level, global/regional
140 offline, and online within ModelE2-YIBs (Yue and Unger, 2015). The offline version is
141 driven with hourly 1°×1° meteorological forcings from either the NASA Modern Era
142 Retrospective-analysis for Research and Applications (MERRA) (Rienecker et al., 2011)
143 or the interpolated output from ModelE2-YIBs. The online YIBs model is coupled with
144 the climate model NASA ModelE2 (Schmidt et al., 2014), which considers the interplay
145 among meteorology, radiation, atmospheric chemistry, and plant photosynthesis at each
146 time step. For both global and regional simulations, 8 plant functional types (PFTs) are
147 considered (Fig. S1). This land cover data set is derived based on retrievals from both the
148 Moderate Resolution Imaging Spectroradiometer (MODIS) (Hansen et al., 2003) and the
149 Advanced Very High Resolution Radiometer (AVHRR) (Defries et al., 2000). The same
150 vegetation cover is used by the Community Land Model (CLM) (Oleson et al., 2010).

151

152 Both the online and offline YIBs models have been extensively evaluated with site-level
153 measurements from 145 globally-dispersed flux tower sites, long-term gridded
154 benchmark products, and multiple satellite retrievals of LAI, tree height, phenology, and



155 carbon fluxes (Yue and Unger, 2015; Yue et al., 2015). Driven with meteorological
156 reanalyses, the offline YIBs vegetation model estimates a global GPP of 122.3 ± 3.1 Pg C
157 yr^{-1} , NPP of 63.6 ± 1.9 Pg C yr^{-1} , and NEE of -2.4 ± 0.7 Pg C yr^{-1} for 1980-2011,
158 consistent with an ensemble of land models (Yue and Unger, 2015). The online
159 simulations with ModelE2-YIBs, including both aerosol effects and O₃ damage, yield a
160 global GPP of 125.8 ± 3.1 Pg C yr^{-1} , NPP of 63.2 ± 0.4 Pg C yr^{-1} , and NEE of -3.0 ± 0.4
161 Pg C yr^{-1} under present day conditions.

162

163 2.2 NASA ModelE2-YIBs model

164

165 The NASA ModelE2-YIBs is a fully coupled chemistry-carbon-climate model with
166 horizontal resolution of $2^\circ \times 2.5^\circ$ latitude by longitude and 40 vertical levels extending to
167 0.1 hPa. The model simulates gas-phase chemistry (NO_x, HO_x, O_x, CO, CH₄, NMVOCs),
168 aerosols (sulfate, nitrate, elemental and organic carbon, dust, sea salt), and their
169 interactions (Schmidt et al., 2014). Modeled oxidants influence the photochemical
170 formation of secondary aerosol species (sulfate, nitrate, secondary organic aerosol). In
171 turn, modeled aerosols affect photolysis rates in the online gas-phase chemistry (Schmidt
172 et al., 2014). Heterogeneous chemistry on dust surfaces is represented (Bauer et al.,
173 2007). The embedded radiation package includes both direct and indirect (Menon and
174 Rotstayn, 2006) radiative effects of aerosols and considers absorption by multiple GHGs.
175 Simulated surface solar radiation exhibits the lowest model-to-observation biases
176 compared with the other 20 IPCC-class climate models (Wild et al., 2013). Simulated
177 meteorological and hydrological variables have been fully validated against observations
178 and reanalysis products (Schmidt et al., 2014).

179

180 2.3 Emissions

181

182 We use global annual anthropogenic pollution inventories from the GAINS integrated
183 assessment model (Amann et al., 2011), which compiles historic emissions of air
184 pollutants for each country based on available international emission inventories and
185 national information from individual countries. Inter-comparison (Fig. S2) shows that the



186 GAINS V4a inventory has similar emission intensity (within $\pm 10\%$) in China as IPCC
187 RCP8.5 scenario (van Vuuren et al., 2011) for most species, except for ammonia, which
188 is higher by 80% in GAINS. The GAINS inventory also projects medium-term variations
189 of future emissions at five-year intervals to the year 2030. The current legislation
190 emissions (CLE) scenario applies full implementation of national legislation affecting air
191 pollution emissions; for China, this represents the 11th five-year plan, including known
192 failures. By 2030, in the CLE inventory, CO decreases by 18%, SO₂ by 21%, black
193 carbon by 28%, and organic carbon by 41%, but NO_x increases by 20%, ammonia by
194 22%, and non-methane volatile organic compounds (NMVOC) by 6%, relative to the
195 2010 emission magnitude in China. To account for potential rapid changes in policy and
196 legislation, we apply the maximum technically feasible reduction (MTFR) emission
197 scenario as the lower limit of future air pollution. The MTFR scenario implements all
198 currently available control technologies, disregarding implementation barriers and costs.
199 With this scenario, the 2030 emissions of NO_x decrease by 76%, CO by 79%, SO₂ by
200 67%, black carbon by 81%, organic carbon by 89%, ammonia by 65%, and NMVOC by
201 62% in China, indicating large improvement of air quality. Biomass burning emissions,
202 adopted from the IPCC RCP8.5 scenario (van Vuuren et al., 2011), decrease by 1-2% for
203 all pollution species at the year 2030 compared with 2010.

204

205 Natural emissions of air pollution show much smaller changes by 2030 compared with
206 anthropogenic emissions. Lightning NO_x emissions increase by $\sim 4\%$ (0.02 Tg N) and soil
207 NO_x emissions increase by $\sim 1\%$ (0.001 Tg N). Emissions of biogenic VOCs, predicted
208 with a photosynthesis-based scheme (Yue et al., 2015), increase by 5% (+0.39 Tg C) for
209 isoprene but decrease by 5% (-0.25 Tg C) for monoterpenes. Changes in natural
210 emissions of SO₂ (volcano and ocean sources) and NH₃ (ocean source) are trivial over
211 China.

212

213 **2.4 Simulations**

214

215 **2.4.1 NASA ModelE2-YIBs online**



216 We perform 24 time-slice simulations to explore the interactive impacts of O₃ and
217 aerosols on land carbon uptake (Table S2). All simulations are performed in atmosphere-
218 only configuration. In these experiments, [O₃] and aerosol loading are dynamically
219 predicted, and atmospheric chemistry processes are fully two-way coupled to the
220 meteorology and the land biosphere. Simulations can be divided into two groups,
221 depending on whether AIE are included. In each group, three subgroups are defined with
222 the emission inventories of GAINS 2010, CLE 2030, and MTRF 2030 scenarios. In each
223 subgroup, one baseline experiment is set up with only natural emissions. The other three
224 implement all natural and anthropogenic sources of emissions, but apply different levels
225 of O₃ damage including none, low sensitivity, and high sensitivity. To compare the
226 differences between online and offline O₃ damage, we perform two additional
227 simulations, G10ALLHO3_OFF and G10ALLLO3_OFF, which do not account for the
228 feedbacks of O₃-induced changes in biometeorology, plant growth, and ecosystem
229 physiology. We use prescribed sea surface temperature (SST) and sea ice distributions
230 simulated by ModelE2 under the IPCC RCP8.5 scenario (van Vuuren et al., 2011). For
231 these boundary conditions, we apply the monthly-varying decadal average of 2006-2015
232 for 2010 simulations and that of 2026-2035 for 2030 simulations. Well-mixed GHG
233 concentrations are also adopted from the RCP8.5 scenario. Land cover change
234 projections for this scenario suggest only minor changes between the years 2010 and
235 2030; for example, the expansion of 3% for grassland is offset by the losses of 1% for
236 cropland and 4% for tropical rainforest. As a result, we elect to apply the same land
237 cover, which is derived from satellite retrievals, for both present-day and future
238 simulations (Fig. S1). We use present-day equilibrium tree height derived from a 30-year
239 spinup procedure (Yue and Unger, 2015) as the initial condition. All simulations are
240 performed for 20 years, and the last 15 years are used for analyses. For simulations
241 including effects of CO₂ fertilization, climate change, and O₃ damages, GPP and NPP
242 reach new equilibrium within 5 years while those for NEE may require several decades
243 due to the slow responses of the soil carbon pools (Fig. S3).

244

245 **2.4.2 YIBs offline with MERRA meteorology**



246 We perform 15 simulations to evaluate the skill of the O₃ damage scheme for vegetation
247 in China (Table S3). Each run is driven with hourly meteorological forcings from NASA
248 GMAO MERRA (Rienecker et al., 2011). One baseline simulation is performed without
249 inclusion of any O₃ damage. The others, seven runs in each of two groups, are driven
250 with fixed [O₃] at 20, 40, 60, 80, 100, 120, and 140 ppbv, respectively, using either low
251 or high O₃ sensitivities defined by (Sitch et al., 2007). Thus, [O₃] in these offline runs is
252 fixed without seasonal and diurnal variations to mimic field experiments that usually
253 apply a constant level of [O₃] during the test period. We compare the O₃-affected GPP
254 with the O₃-free GPP from the baseline simulation to derive the damaging percentages to
255 GPP, which are compared with values for different PFTs from an ensemble of published
256 literature results (Table S1). All simulations are performed for 1995-2011, and the last 10
257 years are used for analyses.

258

259 **2.4.3 YIBs offline with ModelE2-YIBs meteorology**

260 Using the offline YIBs vegetation model driven with ModelE2-YIBs meteorology, we
261 perform 30 simulations to isolate the impacts of aerosol-induced changes in the
262 individual meteorological drivers on carbon uptake (Table S4). Experiments are
263 categorized into two groups, depending on whether the GCM forcings include AIE or
264 not. In each group, three subgroups of simulations are set up with different meteorology
265 for GAINS 2010, CLE 2030, and MTRF 2030 scenarios. Within each subgroup, five runs
266 are designed with the different combinations of GCM forcings. One baseline run is forced
267 with meteorology simulated without anthropogenic aerosols. The other four are
268 additionally driven with aerosol-induced perturbations in temperature, PAR, soil
269 moisture, or the combination of the above three variables. The differences of NPP
270 between sensitivity and baseline runs represent contributions of individual or total aerosol
271 effects. Each simulation is performed for 10 years, with the last 3 years used for analyses.

272

273 **3 Results**

274

275 **3.1 Evaluation of ModelE-YIBs over China**

276



277 **3.1.1 Land carbon fluxes: GPP and NPP**

278 To validate simulated GPP, we use a gridded benchmark product for 2009-2011 upscaled
279 from *in situ* FLUXNET measurements (Jung et al., 2009). For NPP, we use a MODIS
280 satellite-derived product for 2009-2011 (Zhao et al., 2005). Both datasets are interpolated
281 to the same resolution of $2^{\circ} \times 2.5^{\circ}$ as ModelE2-YIBs. Simulated GPP and NPP reproduce
282 the observed spatial patterns with high correlation coefficients ($R=0.46-0.86$, $p < 0.001$)
283 and low model-to-observation biases ($< 20\%$) (Fig. 1 and Fig. S4). High values of the
284 land carbon fluxes are predicted in the East and the Northeast, where forests and
285 croplands dominate (Fig. S1).

286

287 **3.1.2 Surface air pollution and AOD**

288 For surface concentrations of $PM_{2.5}$ and O_3 , we use ground measurements available for
289 2014 from 188 sites operated by the Ministry of Environmental Protection of China
290 (<http://www.aqicn.org/>). In addition, we use rural $[O_3]$ from published literature (Table
291 S5) to evaluate the model. For AOD, we use gridded observations of 2008-2012 from
292 MODIS retrievals. The model simulates reasonable magnitude and spatial distribution of
293 AOD and surface $PM_{2.5}$ concentrations (Fig. 2). Long-term measurements of $[O_3]$ are
294 very limited in China. Comparisons with the 2014 one-year data from 188 urban sites
295 show that simulated $[O_3]$ reproduces reasonable spatial distribution but overestimates the
296 average concentration by $>40\%$. Such discrepancy is in part attributed to the sampling
297 biases, because urban $[O_3]$ is likely lower than rural $[O_3]$ due to high NO_x emissions (NO_x
298 titration) and aerosol loading (light extinction) in cities. Evaluations at rural sites (Table
299 S5) better match the observations that represent the major domain of China (Fig. 3).

300

301 **3.1.3 Shortwave radiation**

302 We use ground-based observations of surface shortwave radiation and diffuse fraction
303 from 106 pyranometer sites managed by the Climate Data Center, Chinese
304 Meteorological Administration (Xia, 2010). Site selection is based on the availability of
305 continuous monthly measurements during 2008-2012, resulting in 95 sites for the
306 evaluation of total shortwave radiation. For diffuse radiation, we select the 17 sites only
307 that provide continuous measurements during 2008-2012. Simulated surface shortwave



308 radiation and diffuse fraction agree well with measurements at 106 sites, especially over
309 the East where low solar insolation while high diffusion are predicted (Fig. 4).

310

311 **3.1.4 Ozone vegetation damage function**

312 We adopt the same approach as Yue et al. (2016) by comparing simulated GPP-to-[O₃]
313 responses (Table S3) with observations from multiple published literature (Table S1). We
314 aggregate these measurements into six categories, including evergreen needleleaf forest
315 (ENF), deciduous broadleaf forest (DBF), shrubland, C3 herbs, C4 herbs, and a mixture
316 of all above species. We derive the sensitivity of GPP to varied [O₃] (Fig. 5) using the
317 YIBs offline version. For most PFTs, simulated O₃ damage increases with [O₃] in broad
318 agreement with measurements. Predicted O₃ damage reproduces observations with a
319 correlation coefficient of 0.61 (for all samplings, $n=32$) and in similar magnitudes (-
320 17.7% vs. -20.4%), suggesting that the damage scheme we adopted from Sitch et al.
321 (2007) is ready to use in China. For the same level of [O₃], deciduous trees suffer larger
322 damages than evergreen trees because the former species are usually more sensitive
323 (Sitch et al., 2007) and have higher g_s (therefore higher uptake) (Wittig et al., 2007).
324 Flux-based O₃ sensitivity for C4 herbs is only half that of C3 herbs (Sitch et al., 2007),
325 however, concentration-based O₃ damages, both observed and simulated, are larger for
326 C4 plants because of their higher uptake efficiency following high g_s (Yue and Unger,
327 2014).

328

329 **3.2 O₃ effects in China**

330

331 We focus our study domain in eastern China (21°-38°N, 102°-122°E, including the North
332 China Plain, the Yangtze River Delta, and part of the Sichuan Basin), a region that suffers
333 from high levels of O₃ and aerosols from anthropogenic pollution sources (>75%
334 contribution; Fig. S5). We estimate that surface O₃ decreases annual GPP in China by
335 10.3% based on YIBs offline simulations in the absence of feedbacks from O₃ vegetation
336 damage to meteorology and plant growth. The damage is stronger in summer, when the
337 average GPP decreases by ~20% for both deciduous trees and C3 herbs in the East (Fig.
338 6). In contrast, a lower average damage to GPP of ~10% is predicted for evergreen



339 needleleaf trees (because of low sensitivity) and C4 herbs (because of the mismatched
340 spatial locations between C4 plants and high [O₃], Fig. S1 and Fig. 2d).

341

342 O₃ damage to photosynthesis can influence plant growth. At the same time, the O₃-
343 induced reductions in stomatal conductance can increase canopy temperature and inhibit
344 plant transpiration (Lombardozzi et al., 2015), leading to surface warming and rainfall
345 deficit (Fig. S6). These biometeorological feedbacks may in turn exacerbate the
346 dampening of land carbon uptake. Application of ModelE2-YIBs that allows for these
347 feedbacks gives an O₃-induced damage to annual GPP of 10.7%, a similar level to the
348 damage computed in YIBs offline. Sensitivity simulations (offline and online) with zero
349 anthropogenic emissions show no O₃ damage, because the [O₃] exposure from natural
350 sources alone is lower than the damaging threshold of 40 ppbv for most PFTs (Fig. 5).
351 Our results indicate that present-day surface O₃ inhibition, averaged for low and high
352 plant sensitivities, reduces total NPP in China by 0.59 ± 0.11 Pg C yr⁻¹ (Table 2),
353 assuming no direct impacts of O₃ on plant respiration.

354

355 **3.3 Aerosol haze effects in China**

356

357 Aerosols decrease direct solar radiation but increase diffuse radiation (Fig. S7), the latter
358 of which is beneficial for canopy photosynthesis. The online coupled model quantifies
359 the concomitant meteorological and hydrological feedbacks (Fig. 7) that further influence
360 the radiative and land carbon fluxes. Reduced insolation decreases summer surface
361 temperature by 0.63°C in the East, inhibiting evaporation but increasing relative humidity
362 (RH) due to lower saturation vapor pressure (Table S6). These feedbacks combine to
363 stimulate photosynthesis (Fig. 8a), which, in turn, strengthens plant transpiration and
364 further increases RH, contributing to enhanced precipitation and cloud cover. Moreover,
365 soil moisture increases with lower evaporation and higher precipitation. Inclusion of AIE
366 results in distinct climatic feedbacks (Fig. S8). The AIE reduces cloud droplet size and
367 inhibits summer precipitation by 0.9 mm day⁻¹ (13%), leading to a 3% decline in soil
368 moisture (Table S6). The AIE also lengthens cloud lifetime and increases cloud cover,
369 further reducing available radiation and causing a stronger surface cooling.



370

371 We separate the relative impacts due to aerosol-induced perturbations in temperature,
372 radiation, and soil moisture (Fig. 8). The overall impact of the aerosol-induced
373 biometeorological feedbacks on the carbon uptake depends on the season and vegetation
374 type. In the summer, the aerosol-induced surface cooling brings leaf temperature closer to
375 the photosynthetic optimum of 25°C, DRF enhances light availability of shaded leaves
376 and LUE of sunlit leaves, and the wetter soil alleviates water stress for stoma.
377 Consequently, aerosol-induced hydroclimatic feedbacks promote ecosystem NPP, albeit
378 with substantial spatiotemporal variability (Fig. 8a and Table 2). Surface cooling
379 enhances NPP in summer (Fig. 8b) but induces neutral net impacts on NPP in spring and
380 autumn (not shown), when leaf temperature is usually below 25°C, because the cooling-
381 driven reductions of photosynthesis are accompanied by simultaneous reductions in plant
382 respiration. Plant phenology is responding to aerosol-induced cooling; however, such
383 changes alone exert much smaller impacts on the ecosystem carbon uptake compared to
384 those driven directly by temperature changes (Yue et al., 2015). We find strong aerosol
385 DRF in the Southeast and the Northeast, where AOD is moderate (Fig. 8c). Over the
386 North China Plain and the Southwest, aerosol DRF is more limited. In these regions, the
387 local background aerosol layer and/or cloud over are sufficiently optically thick that the
388 effect of anthropogenic aerosol pollution is largely to attenuate direct sunlight and reduce
389 NPP (Cohan et al., 2002). Aerosol-induced cooling increases soil moisture over most of
390 the East (Fig. 7f), but the beneficial responses are confined to the Central East (Fig. 8d),
391 where C3 crops dominate (Fig. S1). These short-root plants are more sensitive to short-
392 term water availability than deep-root trees (Beer et al., 2010; Yue et al., 2015).

393

394 In contrast, inclusion of AIE results in detrimental impacts on NPP (Table 2). Aerosol-
395 induced drought strongly reduces regional NPP especially over the Northeast and North
396 China Plain (Fig. S9d), where cropland dominates (Fig. S1). Meanwhile, the increases in
397 cloud cover reduce available radiation, leading to weakened aerosol DRF effects over the
398 Southeast while strengthened NPP reductions in the Southwest (Fig. S9c).

399

400 **3.4 Combined effects of O₃ and aerosol**



401

402 Simultaneous inclusion of the aerosol effects on the land biosphere has negligible impacts
403 on O₃ damage. The online O₃ inhibition, which is much stronger in magnitude than the
404 aerosol effects, shows insignificant differences relative to the offline values (10.7% vs.
405 10.3%). As a result, we consider O₃ and aerosol effects to be linearly additive. In the year
406 2010, the combined effects of O₃ and aerosols decrease total NPP in China by 0.39 to
407 0.80 Pg C yr⁻¹ (Table 2), equivalent to 9-16% of the pollution-free NPP and 16-32% of
408 the total anthropogenic carbon emissions (Liu et al., 2015). A dominant fraction (86%
409 without AIE and 77% with AIE) of the reduced carbon uptake occurs in the East, where
410 dense air pollution is co-located with high NPP (Figs 1 and 2). Independently, O₃ reduces
411 NPP by 0.59 Pg C yr⁻¹, with a large range from 0.43 Pg C yr⁻¹ for low damaging
412 sensitivity to 0.76 Pg C yr⁻¹ for high damaging sensitivity (Table 2). The sign of the
413 aerosol effects is uncertain. Without AIE, aerosol is predicted to increase NPP by 0.2 Pg
414 C yr⁻¹, because of regionally confined DRF effects and enhanced soil moisture (Fig. 8).
415 With inclusion of AIE, aerosol decreases NPP by 0.2 Pg C yr⁻¹, mainly due to reduced
416 soil moisture (Fig. S9). The uncertainty of individual simulations, calculated from the
417 interannual climate variability, is usually smaller than that due to O₃ damage sensitivity
418 and AIE (Table 2).

419

420 **3.5 Future projection of pollution effects**

421

422 Following the CLE scenario, by the year 2030, predicted summer [O₃] increases by 7%,
423 while AOD decreases by 5% and surface PM_{2.5} concentrations decline by 10% (Fig. 9).
424 These changes are predominantly attributed to changes in anthropogenic emissions, as
425 natural sources show limited changes. The reduction of AOD is related to the decreased
426 emissions of SO₂, black carbon, and organic carbon (Fig. S2). In contrast, the
427 enhancement of [O₃] is caused by the increased emissions of NO_x accompanied with the
428 higher air temperature in the warmer 2030 climate. The moderate decline of aerosol
429 loading in the 2030 CLE scenario brings benefits to land ecosystems through DRF effects
430 (Table 2) because light scattering is often saturated in the present-day conditions due to
431 high local AOD and regional cloud cover. Benefits from the aerosol pollution reductions



432 are offset by worsening O₃ vegetation damage in the CLE future world (Fig. 10b). O₃-
433 free ([O₃]=0) NPP increases by 14% in 2030 due to CO₂ fertilization and global climate
434 change. Despite [CO₂] increases from 390 ppm in 2010 to 449 ppm in 2030 in the
435 RCP8.5 scenario (van Vuuren et al., 2011), which drives additional g_s inhibition, the
436 future O₃-induced NPP damage in 2030 degrades to 14% or 0.67 Pg C yr⁻¹ (Table 2).

437

438 The MTRF scenario reflects an ambitious and optimistic future in which there is rapid
439 global implementation of all currently available technological pollution controls. AOD
440 decreases by 55% and [O₃] decreases by 40% for this future scenario (Fig. 9). The model
441 projects much lower damage to NPP of only 0.12 Pg C yr⁻¹ (0.28 Pg C yr⁻¹ with AIE),
442 mainly from the 40% reduction in [O₃] (Fig. 10c). These damages are of similar
443 magnitude to modeling uncertainties (Table 2). The MTRF scenario offers strong
444 recovery of the land carbon uptake in China by 2030.

445

446 **4. Discussion**

447

448 **4.1 Comparison with previous estimates**

449

450 Previous estimates of O₃ damages over the whole China region are very limited. Two
451 important studies, Tian et al. (2011) and Ren et al. (2011), have quantified the impacts of
452 surface O₃ on carbon assimilation in China. Both studies applied the dynamic land
453 ecosystem model (DLEM) with O₃ damage scheme proposed by Felzer et al. (2004),
454 except that Tian et al. (2011) focused on NEE while Ren et al. (2011) also investigated
455 NPP. The Felzer et al. (2004) scheme calculates O₃ uptake based on stomatal
456 conductance and the AOT40 (accumulated hourly O₃ dose over a threshold of 40 ppb).
457 Yue and Unger (2014) estimated O₃-induced reductions in GPP over U.S. using Sitch et
458 al. (2007) scheme and found an average value of 4-8% (low to high sensitivity),
459 consistent with the reduction of 3-7% in Felzer et al. (2004). For this study, we estimate
460 that present-day O₃ decreases NPP by 0.43-0.76 Pg C yr⁻¹, higher than the 0.42 Pg C yr⁻¹
461 calculated by Ren et al. (2011). However, the percentage reduction of 10.1-17.8% in our
462 estimate is weaker than the value of 24.7% in Ren et al. (2011). The main reason for such



463 discrepancy lies in the differences in the climatological NPP. Combining all
464 environmental drivers (e.g. [CO₂], meteorology, [O₃], and aerosols), we predict an
465 average NPP of 3.98 ± 0.1 Pg C yr⁻¹ for the year 2010 (uncertainties from AIE) with the
466 ModelE2-YIBs model. This value is close to the average of 3.35 ± 1.25 Pg C yr⁻¹ for
467 1981-2000 calculated based on 54 estimates from 33 studies (Shao et al., 2016). Using
468 DLEM, Ren et al. (2011) estimated an optimal NPP of 1.67 Pg C yr⁻¹ for 2000-2005 over
469 China, which is only half of the literature-based estimate.

470

471 In the absence of any previous studies of aerosol pollution effects on land carbon uptake
472 in China, our strategy is to compare separately the simulated aerosol climatic feedback
473 (climate sensitivity) and simulated NPP response to climate variability (NPP sensitivity)
474 with existing published results. ModelE2-YIBs simulates an annual reduction of 26.2 W
475 m⁻² in all-sky surface solar radiation over the East due to aerosols pollution (Table S6),
476 similar to the estimate of 28 W m⁻² by Folini and Wild (2015). In response to this
477 radiative perturbation, aerosol pollution causes a widespread cooling of 0.3-0.9 °C in
478 summer over the East (Fig. 7a), consistent with estimates of 0-0.9 °C by Qian et al.
479 (2003), 0-0.7 °C by Liu et al. (2009), and average of 0.5 °C by Folini and Wild (2015).
480 Aerosol pollution effects on regional precipitation patterns in China are not well
481 understood due to different climate model treatments of land-atmosphere interactions and
482 the interplay between regional and large-scale circulation. In ModelE2-YIBs, without
483 AIE, aerosol induces a “northern drought and southern flood” pattern in agreement with
484 Gu et al. (2006), but different to Liu et al. (2009) who predicted widespread drought
485 instead. Including both aerosol direct and indirect effects, ModelE2-YIBs simulates an
486 average reduction of 0.48 mm day⁻¹ in summer rainfall widespread over China (Fig. S8b),
487 similar to the magnitude of 0.4 mm day⁻¹ estimated with the ECHAM5-HAM model
488 (Folini and Wild, 2015), but higher than the 0.21 mm day⁻¹ predicted by the RegCM2
489 model (Huang et al., 2007).

490

491 Sensitivity experiments with YIBs show that summer NPP increases following aerosol-
492 induced changes in temperature, radiation, and precipitation (Fig. 8). The cooling-related
493 NPP enhancement (Fig. 8b) collocates with changes in temperature (Fig. 7a), indicating



494 that sensitivity of NPP to temperature is negative over eastern China. Such temperature
495 sensitivity is consistent with the ensemble estimate based on 10 terrestrial models (Piao et
496 al., 2013). For the aerosol-induced radiative perturbation, many studies have shown that
497 moderate aerosol/cloud amount promotes plant photosynthesis through enhanced DRF,
498 while dense aerosol/cloud decreases carbon uptake due to light extinction (Cohan et al.,
499 2002; Gu et al., 2003; Rocha et al., 2004; Alton, 2008; Knohl and Baldocchi, 2008;
500 Mercado et al., 2009; Jing et al., 2010; Bai et al., 2012; Cirino et al., 2014; Strada et al.,
501 2015). Theoretically, at each specific land location on the Earth, there is an AOD
502 threshold below which aerosol promotes local NPP. The threshold is dependent on
503 latitude, cloud/aerosol amount, and plant types. In a related study by Yue and Unger
504 (2016), we applied a well-validated offline radiation model to calculate these AOD
505 thresholds over China. We conclude that present-day AOD is lower than the local
506 thresholds in the Northeast and Southeast but exceeds the thresholds in the North China
507 Plain, explaining why aerosol-induced dimming enhances NPP in the former regions but
508 reduces NPP in the latter (Fig. 8c). On the country level, the NPP enhancement due to
509 aerosol DRF is $0.07 \text{ Pg C yr}^{-1}$ in Yue and Unger (2016), very close to the $0.09 \text{ Pg C yr}^{-1}$
510 estimated with ModelE2-YIBs model (Table 2).

511

512 **4.2 Uncertainties**

513

514 A major source of uncertainty originates from the paucity of observations. For instance,
515 direct measurements of aerosol pollution effects on NPP are non-existent for China. The
516 aerosol effects involve complex interactions that challenge the field-based validation of
517 the underlying independent processes. Field experiments of O_3 vegetation damage are
518 becoming more available, but their applications are limited by the large variations in the
519 species-specific responses (Lombardozzi et al., 2013), as well as the discrepancies in the
520 treatments of $[\text{O}_3]$ enhancement (Wittig et al., 2007). Instead of equally using all
521 individual records from multiple literatures (Lombardozzi et al., 2013), we aggregate O_3
522 damage for each literature based on the seasonal (or growth-season) average. In this way,
523 the derived PFT-level GPP- $[\text{O}_3]$ relationships are not biased towards the experiments



524 with a large number of samplings. Such aggregation also reduces sampling noise and
525 allows construction of the quantified GPP-[O₃] relationships used for model assessment.

526

527 We have estimated O₃ damages to NPP (instead of GPP), an optimal indicator for net
528 carbon uptake by plants. Our calculations assume no impacts of O₃ on autotrophic
529 respiration. Yet, limited observations have found increased plant respiration in response
530 to O₃ injury (Felzer et al., 2007), suggesting that our calculation of O₃-induced NPP
531 reductions might be underestimated. Current large mechanistic uncertainties in the role of
532 anthropogenic nitrogen (N) deposition to China's land carbon uptake (Tian et al., 2011;
533 Xiao et al., 2015) have prohibited the inclusion of dynamic carbon-nitrogen coupling in
534 the Earth system model used here. Previous studies have suggested that inclusion of N
535 fertilization can relieve or offset damages by O₃, especially for N-limited forests
536 (Ollinger et al., 2002). Relative to the present day, atmospheric reactive N deposition
537 increases by 20% in the CLE scenario but decreases by 60% in the MTFR scenario,
538 suggesting that the stronger O₃ damage in CLE might be overestimated while the reduced
539 damage in MTFR might be too optimistic. Furthermore, the relatively coarse resolution
540 of the global model, usage of emission inventories, selection of aerosol parameters, and
541 application of AIE may introduce additional biases and exacerbate the total uncertainties.

542

543 Importantly, our estimate of NPP response to aerosol effects, with or without AIE, is
544 secondary in magnitude compared with the O₃ vegetation damage, suggesting that the net
545 impact of current air pollution levels in China is detrimental to the land carbon uptake
546 there. Locally, this pollution damage exerts a threat to plant health, terrestrial ecosystem
547 services, and food production. Globally, air pollution effects may enhance planetary
548 warming by decreasing the land removal rate of atmospheric CO₂. Our results show
549 substantial benefits to the protection of plant health and the regional land carbon sink in
550 China from stringent air pollution controls, especially for O₃ precursors. Our analysis
551 highlights the complex interplay between immediate and more local pollution issues, and
552 longer-term global warming. Future air pollution controls provide an additional co-
553 benefit to human society: the offsetting of fossil fuel CO₂ emissions through enhanced
554 land sequestration of atmospheric CO₂.



555

556 *Acknowledgements.* X. Yue acknowledges funding support from “Thousand Youth
557 Talents Plan”. This research was supported in part by the facilities and staff of the Yale
558 University Faculty of Arts and Sciences High Performance Computing Center.

559

560 **References**

- 561 Ainsworth, E. A., Yendrek, C. R., Sitch, S., Collins, W. J., and Emberson, L. D.: The
562 Effects of Tropospheric Ozone on Net Primary Productivity and Implications for
563 Climate Change, *Annual Review of Plant Biology*, Vol 63, 63, 637-661,
564 doi:10.1146/Annurev-Arplant-042110-103829, 2012.
- 565 Alton, P. B.: Reduced carbon sequestration in terrestrial ecosystems under overcast skies
566 compared to clear skies, *Agricultural and Forest Meteorology*, 148, 1641–1653,
567 doi:10.1016/j.agrformet.2008.05.014, 2008.
- 568 Amann, M., Bertok, I., Borken-Kleefeld, J., Cofala, J., Heyes, C., Hoglund-Isaksson, L.,
569 Klimont, Z., Nguyen, B., Posch, M., Rafaj, P., Sandler, R., Schopp, W., Wagner, F.,
570 and Winiwarter, W.: Cost-effective control of air quality and greenhouse gases in
571 Europe: Modeling and policy applications, *Environmental Modelling & Software*,
572 26, 1489-1501, doi:10.1016/j.envsoft.2011.07.012, 2011.
- 573 Bai, Y., Wang, J., Zhang, B., Zhang, Z., and Liang, J.: Comparing the impact of
574 cloudiness on carbon dioxide exchange in a grassland and a maize cropland in
575 northwestern China, *Ecological Research*, 27, 615-623, doi:10.1007/s11284-012-
576 0930-z, 2012.
- 577 Ball, J. T., Woodrow, I. E., and Berry, J. A.: A model predicting stomatal conductance
578 and its contribution to the control of photosynthesis under different environmental
579 conditions, in: *Progress in Photosynthesis Research*, edited by: Biggins, J., Nijhoff,
580 Dordrecht, Netherlands, 110–112, 1987.
- 581 Bauer, S. E., Mishchenko, M. I., Lacic, A. A., Zhang, S., Perlwitz, J., and Metzger, S. M.:
582 Do sulfate and nitrate coatings on mineral dust have important effects on radiative
583 properties and climate modeling?, *Journal of Geophysical Research*, 112, D06307
584 doi:10.1029/2005JD006977, 2007.
- 585 Beer, C., Reichstein, M., Tomelleri, E., Ciais, P., Jung, M., Carvalhais, N., Rodenbeck,
586 C., Arain, M. A., Baldocchi, D., Bonan, G. B., Bondeau, A., Cescatti, A., Lasslop,
587 G., Lindroth, A., Lomas, M., Luysaert, S., Margolis, H., Oleson, K. W., Rouspard,
588 O., Veenendaal, E., Viovy, N., Williams, C., Woodward, F. I., and Papale, D.:
589 Terrestrial Gross Carbon Dioxide Uptake: Global Distribution and Covariation with
590 Climate, *Science*, 329, 834-838, doi:10.1126/Science.1184984, 2010.
- 591 Cirino, G. G., Souza, R. A. F., Adams, D. K., and Artaxo, P.: The effect of atmospheric
592 aerosol particles and clouds on net ecosystem exchange in the Amazon, *Atmospheric
593 Chemistry and Physics*, 14, 6523-6543, doi:10.5194/acp-14-6523-2014, 2014.
- 594 Cohan, D. S., Xu, J., Greenwald, R., Bergin, M. H., and Chameides, W. L.: Impact of
595 atmospheric aerosol light scattering and absorption on terrestrial net primary
596 productivity, *Global Biogeochemical Cycles*, 16, 1090, doi:10.1029/2001gb001441,
597 2002.
- 598 Defries, R. S., Hansen, M. C., Townshend, J. R. G., Janetos, A. C., and Loveland, T. R.:
599 A new global 1-km dataset of percentage tree cover derived from remote sensing,
600 *Global Change Biology*, 6, 247-254, doi:10.1046/J.1365-2486.2000.00296.X, 2000.
- 601 Farquhar, G. D., Caemmerer, S. V., and Berry, J. A.: A Biochemical-Model of
602 Photosynthetic Co₂ Assimilation in Leaves of C-3 Species, *Planta*, 149, 78-90,
603 doi:10.1007/Bf00386231, 1980.
- 604 Felzer, B., Kicklighter, D., Melillo, J., Wang, C., Zhuang, Q., and Prinn, R.: Effects of
605 ozone on net primary production and carbon sequestration in the conterminous



- 606 United States using a biogeochemistry model, *Tellus Series B-Chemical and*
607 *Physical Meteorology*, 56, 230-248, doi:Doi 10.1111/J.1600-0889.2004.00097.X,
608 2004.
- 609 Felzer, B. S., Cronin, T., Reilly, J. M., Melillo, J. M., and Wang, X.: Impacts of ozone on
610 trees and crops, *C. R. Geoscience*, 229, doi:10.1016/j.crte.2007.08.008, 2007.
- 611 Folini, D., and Wild, M.: The effect of aerosols and sea surface temperature on China's
612 climate in the late twentieth century from ensembles of global climate simulations, *J.*
613 *Geophys. Res.*, 12, 2261-2279, doi:10.1002/2014JD022851, 2015.
- 614 Gu, L. H., Baldocchi, D. D., Wofsy, S. C., Munger, J. W., Michalsky, J. J., Urbanski, S.
615 P., and Boden, T. A.: Response of a deciduous forest to the Mount Pinatubo
616 eruption: Enhanced photosynthesis, *Science*, 299, 2035-2038,
617 doi:10.1126/science.1078366, 2003.
- 618 Gu, Y., Liou, K. N., Xue, Y., Mechoso, C. R., Li, W., and Luo, Y.: Climatic effects of
619 different aerosol types in China simulated by the UCLA general circulation model,
620 *Journal of Geophysical Research*, 111, D15201, doi:10.1029/2005JD006312, 2006.
- 621 Hansen, M. C., DeFries, R. S., Townshend, J. R. G., Carroll, M., Dimiceli, C., and
622 Sohlberg, R. A.: Global Percent Tree Cover at a Spatial Resolution of 500 Meters:
623 First Results of the MODIS Vegetation Continuous Fields Algorithm, *Earth*
624 *Interactions*, 7, 1-15, doi:10.1175/1087-3562(2003)007<0001:GPTCAA>2.0.CO;2,
625 2003.
- 626 Huang, Y., Chameides, W. L., and Dickinson, R. E.: Direct and indirect effects of
627 anthropogenic aerosols on regional precipitation over east Asia, *Journal of*
628 *Geophysical Research*, 112, D03212, doi:10.1029/2006JD007114, 2007.
- 629 Jing, X., Huang, J., Wang, G., Higuchi, K., Bi, J., Sun, Y., Yu, H., and Wang, T.: The
630 effects of clouds and aerosols on net ecosystem CO₂ exchange over semi-arid Loess
631 Plateau of Northwest China, *Atmospheric Chemistry and Physics*, 10, 8205-8218,
632 doi:10.5194/acp-10-8205-2010, 2010.
- 633 Jung, M., Reichstein, M., and Bondeau, A.: Towards global empirical upscaling of
634 FLUXNET eddy covariance observations: validation of a model tree ensemble
635 approach using a biosphere model, *Biogeosciences*, 6, 2001-2013, doi:10.5194/bg-6-
636 2001-2009, 2009.
- 637 Kanniah, K. D., Beringer, J., North, P., and Hutley, L.: Control of atmospheric particles
638 on diffuse radiation and terrestrial plant productivity: A review, *Progress in Physical*
639 *Geography*, 36, 209-237, doi:10.1177/0309133311434244, 2012.
- 640 Knohl, A., and Baldocchi, D. D.: Effects of diffuse radiation on canopy gas exchange
641 processes in a forest ecosystem, *Journal of Geophysical Research*, 113, G02023,
642 doi:10.1029/2007JG000663, 2008.
- 643 Liu, Y., Sun, J., and Yang, B.: The effects of black carbon and sulphate aerosols in China
644 regions on East Asia monsoons, *Tellus Series B-Chemical and Physical*
645 *Meteorology*, 61B, 642-656, doi:10.1111/j.1600-0889.2009.00427.x, 2009.
- 646 Liu, Z., Guan, D. B., Wei, W., Davis, S. J., Ciais, P., Bai, J., Peng, S. S., Zhang, Q.,
647 Hubacek, K., Marland, G., Andres, R. J., Crawford-Brown, D., Lin, J. T., Zhao, H.
648 Y., Hong, C. P., Boden, T. A., Feng, K. S., Peters, G. P., Xi, F. M., Liu, J. G., Li, Y.,
649 Zhao, Y., Zeng, N., and He, K. B.: Reduced carbon emission estimates from fossil
650 fuel combustion and cement production in China, *Nature*, 524, 335-338,
651 doi:10.1038/nature14677, 2015.



- 652 Lombardozzi, D., Sparks, J. P., and Bonan, G.: Integrating O₃ influences on terrestrial
653 processes: photosynthetic and stomatal response data available for regional and
654 global modeling, *Biogeosciences*, 10, 6815-6831, doi:10.5194/bg-10-6815-2013,
655 2013.
- 656 Lombardozzi, D., Levis, S., Bonan, G., Hess, P. G., and Sparks, J. P.: The Influence of
657 Chronic Ozone Exposure on Global Carbon and Water Cycles, *Journal of Climate*,
658 28, 292-305, doi:10.1175/Jcli-D-14-00223.1, 2015.
- 659 Menon, S., and Rotstayn, L.: The radiative influence of aerosol effects on liquid-phase
660 cumulus and stratiform clouds based on sensitivity studies with two climate models,
661 *Climate Dynamics*, 27, 345-356, doi:10.1007/s00382-006-0139-3, 2006.
- 662 Mercado, L. M., Bellouin, N., Sitch, S., Boucher, O., Huntingford, C., Wild, M., and
663 Cox, P. M.: Impact of changes in diffuse radiation on the global land carbon sink,
664 *Nature*, 458, 1014-1017, doi:10.1038/Nature07949, 2009.
- 665 Oleson, K. W., Lawrence, D. M., Bonan, G. B., Flanner, M. G., Kluzek, E., Lawrence, P.
666 J., Levis, S., Swenson, S. C., and Thornton, P. E.: Technical Description of version
667 4.0 of the Community Land Model (CLM), National Center for Atmospheric
668 Research, Boulder, CONCAR/TN-478+STR, 2010.
- 669 Ollinger, S. V., Aber, J. D., Reich, P. B., and Freuder, R. J.: Interactive effects of
670 nitrogen deposition, tropospheric ozone, elevated CO₂ and land use history on the
671 carbon dynamics of northern hardwood forests, *Global Change Biology*, 8, 545-562,
672 doi:10.1046/J.1365-2486.2002.00482.X, 2002.
- 673 Piao, S. L., Fang, J. Y., Ciais, P., Peylin, P., Huang, Y., Sitch, S., and Wang, T.: The
674 carbon balance of terrestrial ecosystems in China, *Nature*, 458, 1009-1013,
675 doi:10.1038/nature07944, 2009.
- 676 Piao, S. L., Sitch, S., Ciais, P., Friedlingstein, P., Peylin, P., Wang, X. H., Ahlstrom, A.,
677 Anav, A., Canadell, J. G., Cong, N., Huntingford, C., Jung, M., Levis, S., Levy, P.
678 E., Li, J. S., Lin, X., Lomas, M. R., Lu, M., Luo, Y. Q., Ma, Y. C., Myneni, R. B.,
679 Poulter, B., Sun, Z. Z., Wang, T., Viovy, N., Zaehle, S., and Zeng, N.: Evaluation of
680 terrestrial carbon cycle models for their response to climate variability and to CO₂
681 trends, *Global Change Biology*, 19, 2117-2132, doi:10.1111/Gcb.12187, 2013.
- 682 Qian, Y., Leung, L. R., Ghan, S. J., and Giorgi, F.: Regional climate effects of aerosols
683 over China: modeling and observation, *Tellus Series B-Chemical and Physical
684 Meteorology*, 55, 914-934, doi:10.1046/j.1435-6935.2003.00070.x, 2003.
- 685 Reich, P. B., and Amundson, R. G.: Ambient Levels of Ozone Reduce Net
686 Photosynthesis in Tree and Crop Species, *Science*, 230, 566-570,
687 doi:10.1126/science.230.4725.566, 1985.
- 688 Ren, W., Tian, H., Tao, B., Chappelka, A., Sun, G., Lu, C., Liu, M., Chen, G., and Xu,
689 X.: Impacts of tropospheric ozone and climate change on net primary productivity
690 and net carbon exchange of China's forest ecosystems, *Global Ecology &
691 Biogeography*, 20, 391-406, doi:10.1111/j.1466-8238.2010.00606.x, 2011.
- 692 Rienecker, M. M., Suarez, M. J., Gelaro, R., Todling, R., Bacmeister, J., Liu, E.,
693 Bosilovich, M. G., Schubert, S. D., Takacs, L., Kim, G. K., Bloom, S., Chen, J. Y.,
694 Collins, D., Conaty, A., Da Silva, A., Gu, W., Joiner, J., Koster, R. D., Lucchesi, R.,
695 Molod, A., Owens, T., Pawson, S., Pegion, P., Redder, C. R., Reichle, R., Robertson,
696 F. R., Ruddick, A. G., Sienkiewicz, M., and Woollen, J.: MERRA: NASA's Modern-



- 697 Era Retrospective Analysis for Research and Applications, *Journal of Climate*, 24,
698 3624-3648, doi:10.1175/Jcli-D-11-00015.1, 2011.
- 699 Rocha, A. V., Su, H. B., Vogel, C. S., Schmid, H. P., and Curtis, P. S.: Photosynthetic
700 and water use efficiency responses to diffuse radiation by an aspen-dominated
701 northern hardwood forest, *Forest Science*, 50, 793-801, 2004.
- 702 Schaefer, K., Schwalm, C. R., Williams, C., Arain, M. A., Barr, A., Chen, J. M., Davis,
703 K. J., Dimitrov, D., Hilton, T. W., Hollinger, D. Y., Humphreys, E., Poulter, B.,
704 Raczka, B. M., Richardson, A. D., Sahoo, A., Thornton, P., Vargas, R., Verbeeck,
705 H., Anderson, R., Baker, I., Black, T. A., Bolstad, P., Chen, J. Q., Curtis, P. S.,
706 Desai, A. R., Dietze, M., Dragoni, D., Gough, C., Grant, R. F., Gu, L. H., Jain, A.,
707 Kucharik, C., Law, B., Liu, S. G., Lokipitiya, E., Margolis, H. A., Matamala, R.,
708 McCaughey, J. H., Monson, R., Munger, J. W., Oechel, W., Peng, C. H., Price, D.
709 T., Ricciuto, D., Riley, W. J., Roulet, N., Tian, H. Q., Tonitto, C., Torn, M., Weng,
710 E. S., and Zhou, X. L.: A model-data comparison of gross primary productivity:
711 Results from the North American Carbon Program site synthesis, *J. Geophys. Res.*,
712 117, G03010, doi:10.1029/2012jg001960, 2012.
- 713 Schmidt, G. A., Kelley, M., Nazarenko, L., Ruedy, R., Russell, G. L., Aleinov, I., Bauer,
714 M., Bauer, S. E., Bhat, M. K., Bleck, R., Canuto, V., Chen, Y. H., Cheng, Y., Clune,
715 T. L., Del Genio, A., de Fainchtein, R., Faluvegi, G., Hansen, J. E., Healy, R. J.,
716 Kiang, N. Y., Koch, D., Lacis, A. A., LeGrande, A. N., Lerner, J., Lo, K. K.,
717 Matthews, E. E., Menon, S., Miller, R. L., Oinas, V., Oloso, A. O., Perlwitz, J. P.,
718 Puma, M. J., Putman, W. M., Rind, D., Romanou, A., Sato, M., Shindell, D. T., Sun,
719 S., Syed, R. A., Tausnev, N., Tsigaridis, K., Unger, N., Voulgarakis, A., Yao, M. S.,
720 and Zhang, J. L.: Configuration and assessment of the GISS ModelE2 contributions
721 to the CMIP5 archive, *Journal of Advances in Modeling Earth Systems*, 6, 141-184,
722 doi:10.1002/2013ms000265, 2014.
- 723 Shao, J., Zhou, X. H., Luo, Y. Q., Zhang, G. D., Yan, W., Li, J. X., Li, B., Dan, L.,
724 Fisher, J. B., Gao, Z. Q., He, Y., Huntzinger, D., Jain, A. K., Mao, J. F., Meng, J. H.,
725 Michalak, A. M., Parazoo, N. C., Peng, C. H., Poulter, B., Schwalm, C. R., Shi, X.
726 Y., Sun, R., Tao, F. L., Tian, H. Q., Wei, Y. X., Zeng, N., Zhu, Q., and Zhu, W. Q.:
727 Uncertainty analysis of terrestrial net primary productivity and net biome
728 productivity in China during 1901-2005, *Journal of Geophysical Research*, 121,
729 1372-1393, doi:10.1002/2015jg003062, 2016.
- 730 Sitch, S., Cox, P. M., Collins, W. J., and Huntingford, C.: Indirect radiative forcing of
731 climate change through ozone effects on the land-carbon sink, *Nature*, 448, 791-794,
732 doi:10.1038/Nature06059, 2007.
- 733 Spitters, C. J. T.: Separating the Diffuse and Direct Component of Global Radiation and
734 Its Implications for Modeling Canopy Photosynthesis .2. Calculation of Canopy
735 Photosynthesis, *Agricultural and Forest Meteorology*, 38, 231-242,
736 doi:10.1016/0168-1923(86)90061-4, 1986.
- 737 Spracklen, D. V., Arnold, S. R., and Taylor, C. M.: Observations of increased tropical
738 rainfall preceded by air passage over forests, *Nature*, 489, 282-285,
739 doi:10.1038/nature11390, 2012.
- 740 Steiner, A. L., and Chameides, W. L.: Aerosol-induced thermal effects increase modelled
741 terrestrial photosynthesis and transpiration, *Tellus Series B-Chemical and Physical
742 Meteorology*, 57, 404-411, doi:DOI 10.1111/j.1600-0889.2005.00158.x, 2005.



- 743 Strada, S., Unger, N., and Yue, X.: Observed aerosol-induced radiative effect on plant
744 productivity in the eastern United States, *Atmospheric Environment*, 122, 463–476,
745 doi:10.1016/j.atmosenv.2015.09.051, 2015.
- 746 Tian, H. Q., Melillo, J., Lu, C. Q., Kicklighter, D., Liu, M. L., Ren, W., Xu, X. F., Chen,
747 G. S., Zhang, C., Pan, S. F., Liu, J. Y., and Running, S.: China's terrestrial carbon
748 balance: Contributions from multiple global change factors, *Global Biogeochemical
749 Cycles*, 25, Gb1007, doi:10.1029/2010gb003838, 2011.
- 750 van Vuuren, D. P., Edmonds, J., Kainuma, M., Riahi, K., Thomson, A., Hibbard, K.,
751 Hurtt, G. C., Kram, T., Krey, V., Lamarque, J. F., Masui, T., Meinshausen, M.,
752 Nakicenovic, N., Smith, S. J., and Rose, S. K.: The representative concentration
753 pathways: an overview, *Climatic Change*, 109, 5-31, doi:10.1007/s10584-011-0148-
754 z, 2011.
- 755 Wild, M., Folini, D., Schar, C., Loeb, N., Dutton, E. G., and Konig-Langlo, G.: The
756 global energy balance from a surface perspective, *Climate Dynamics*, 40, 3107-3134,
757 doi:10.1007/s00382-012-1569-8, 2013.
- 758 Wittig, V. E., Ainsworth, E. A., and Long, S. P.: To what extent do current and projected
759 increases in surface ozone affect photosynthesis and stomatal conductance of trees?
760 A meta-analytic review of the last 3 decades of experiments, *Plant Cell and
761 Environment*, 30, 1150-1162, doi:10.1111/J.1365-3040.2007.01717.X, 2007.
- 762 Xia, X.: A closer looking at dimming and brightening in China during 1961-2005,
763 *Annales Geophysicae*, 28, 1121-1132, doi:10.5194/angeo-28-1121-2010, 2010.
- 764 Xiao, J. F., Zhou, Y., and Zhang, L.: Contributions of natural and human factors to
765 increases in vegetation productivity in China, *Ecosphere*, 6, 233, doi:10.1890/Es14-
766 00394.1, 2015.
- 767 Yue, X., and Unger, N.: Ozone vegetation damage effects on gross primary productivity
768 in the United States, *Atmospheric Chemistry and Physics*, 14, 9137-9153,
769 doi:10.5194/acp-14-9137-2014, 2014.
- 770 Yue, X., and Unger, N.: The Yale Interactive terrestrial Biosphere model version 1.0:
771 description, evaluation and implementation into NASA GISS ModelE2,
772 *Geoscientific Model Development*, 8, 2399-2417, doi:10.5194/gmd-8-2399-2015,
773 2015.
- 774 Yue, X., Unger, N., and Zheng, Y.: Distinguishing the drivers of trends in land carbon
775 fluxes and biogenic emissions over the past three decades, *Atmospheric Chemistry
776 and Physics*, 15, 11931-11948, doi:10.5194/acp-15-11931-2015, 2015.
- 777 Yue, X., Keenan, T. F., Munger, W., and Unger, N.: Limited effect of ozone reductions
778 on the 20-year photosynthesis trend at Harvard forest, *Global Change Biology*, 22,
779 3750-3759, doi:10.1111/gcb.13300, 2016.
- 780 Yue, X., and Unger, N.: Aerosol pollution radiative effects on land carbon uptake in
781 China, *Atmospheric Chemistry and Physics Discussion*, in review, doi:10.5194/acp-
782 2016-899, 2016.
- 783 Zhao, M. S., Heinsch, F. A., Nemani, R. R., and Running, S. W.: Improvements of the
784 MODIS terrestrial gross and net primary production global data set, *Remote Sensing
785 of Environment*, 95, 164-176, doi:10.1016/J.Rse.2004.12.011, 2005.
- 786
787



788

789

790 **Table 1.** Summary of models and simulations

791

Model Name	Model class	Climate drivers	Number of runs	Table index ^a	Purpose
ModelE2-YIBs	Coupled climate model	Online	24	S2	Calculate Δ NPP by O ₃ and aerosols at 2010 and 2030
YIBs	Vegetation model	MERRA	15	S3	Evaluate O ₃ damage scheme for China PFTs
YIBs	Vegetation model	ModelE2-YIBs	30	S4	Isolate aerosol individual climatic impacts on NPP

792

793 ^a Table index refers to the tables in supporting information.



794

795

796 **Table 2.** Changes in NPP over China due to combined and separate effects ^a of air
 797 pollution (units: Pg C yr⁻¹)

798

	2010	2030 CLE	2030 MTRF
O₃ (mean) ^b	-0.59 ± 0.11 (-0.60 ± 0.13)	-0.67 ± 0.11 (-0.71 ± 0.16)	-0.29 ± 0.14 (-0.31 ± 0.10)
Low sensitivity	-0.43 ± 0.12 (-0.40 ± 0.13)	-0.43 ± 0.14 (-0.51 ± 0.16)	-0.22 ± 0.17 (-0.15 ± 0.10)
High sensitivity	-0.76 ± 0.15 (-0.80 ± 0.16)	-0.90 ± 0.13 (-0.92 ± 0.18)	-0.36 ± 0.16 (-0.46 ± 0.12)
Aerosol (total) ^c	0.20 ± 0.08 (-0.20 ± 0.09)	0.23 ± 0.14 (-0.09 ± 0.19)	0.16 ± 0.14 (0.04 ± 0.17)
Temperature ^d	0.03 ± 0.04 (0.01 ± 0.04)	0.04 ± 0.02 (0.02 ± 0.05)	0.03 ± 0.04 (0.00 ± 0.04)
Radiation ^d	0.09 ± 0.04 (-0.03 ± 0.04)	0.16 ± 0.06 (-0.01 ± 0.06)	0.11 ± 0.04 (-0.03 ± 0.03)
Soil moisture ^d	0.07 ± 0.07 (-0.19 ± 0.10)	0.01 ± 0.09 (-0.09 ± 0.15)	0.03 ± 0.12 (0.00 ± 0.09)
O₃ + aerosol (net)	-0.39 ± 0.12 (-0.80 ± 0.11)	-0.43 ± 0.12 (-0.80 ± 0.10)	-0.12 ± 0.13 (-0.28 ± 0.14)

799

800 ^a Results shown are the averages ± one standard deviation. Simulations with both aerosol
 801 direct and indirect radiative effects (AIE) are shown in the brackets.

802 ^b Uncertainties for mean O₃ damages are calculated as half of differences in ΔNPP
 803 between low and high sensitivities.

804 ^c Combined aerosol effects are calculated with the ModelE2-YIBs climate model.

805 ^d Separate aerosol effects are calculated with the offline YIBs vegetation model driven
 806 with forcings from the climate model (Table S4).

807

808

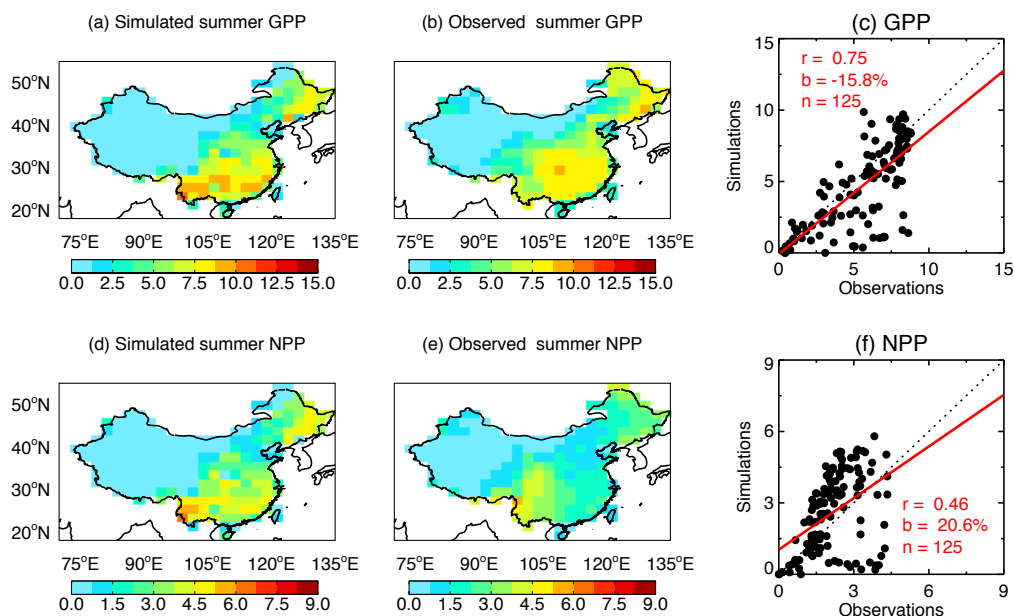
809

810

811

812

813



814

815

816 **Figure 1.** Evaluation of simulated summertime carbon fluxes by ModelE2-YIBs. Panels
 817 show GPP (top row) and NPP (bottom row) over China. Simulation results (a, d) are the
 818 average of G10ALLHO3 and G10ALLLO3, which are performed with the climate model
 819 ModelE2-YIBs using high and low ozone damage sensitivities (Table S2). The
 820 correlation coefficients (r), relative biases (b), and number of grid cells (n) for the
 821 comparisons are listed on the scatter plots. Units: $\text{g C m}^{-2} \text{ day}^{-1}$.

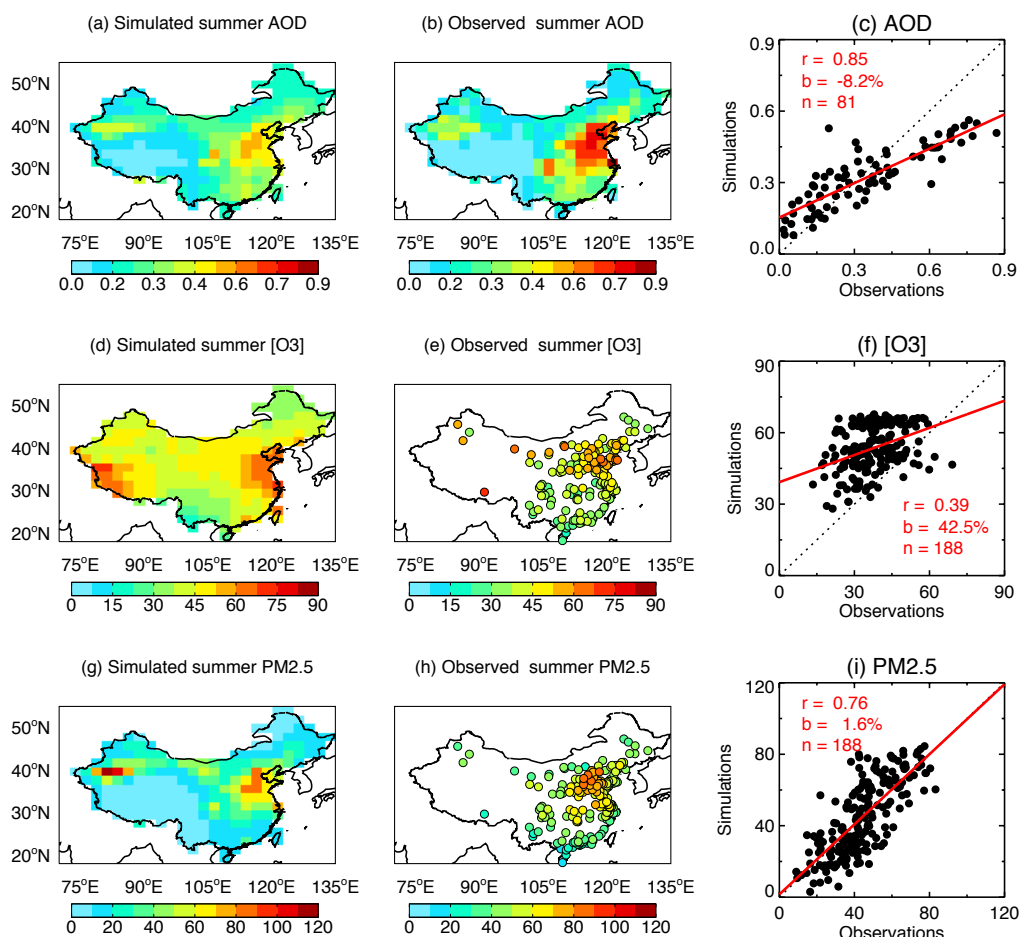
822

823

824



825
826

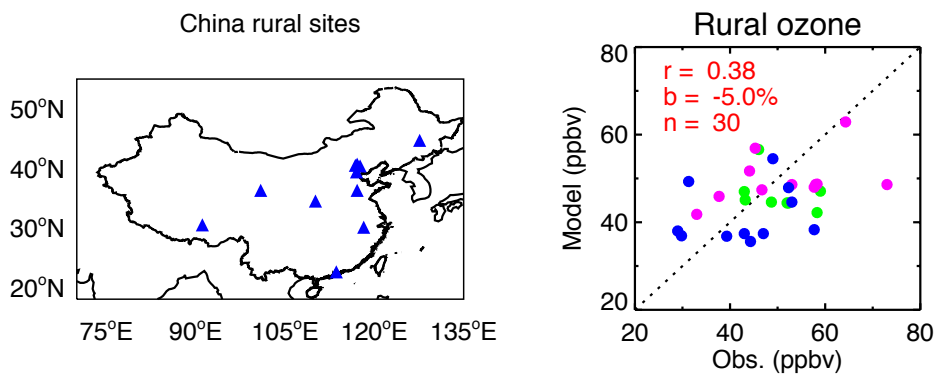


827
828
829
830
831
832
833
834
835
836
837

Figure 2. Evaluation of simulated summertime air pollution in China. Evaluations shown include (a) aerosol optical depth (AOD) at 550 nm, (d) $[O_3]$ (units: ppbv), and (g) $PM_{2.5}$ concentrations (units: $\mu g m^{-3}$) with observations from (b) the satellite retrieval of the MODIS, and (e) and (h) measurements from 188 ground-based sites. Simulation results are from G10ALLNO3 performed with the climate model ModelE2-YIBs (Table S2). The correlation coefficients (r), relative biases (b), and number of sites/grids (n) for the comparisons are listed on the scatter plots.



838
839

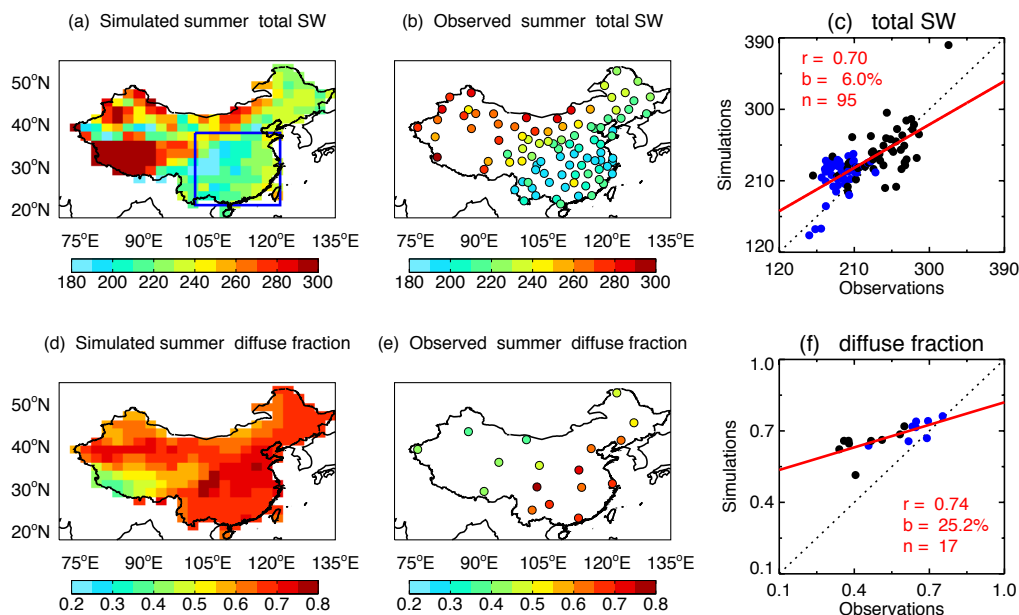


840
841 **Figure 3.** Evaluation of simulated [O₃] at rural sites in China. Simulation results are from
842 G10ALLNO3 performed with the climate model NASA ModelE2-YIBs (Table S2). For
843 the scatter plots, green, pink, and blue points represent values in spring, summer, and
844 autumn, respectively. The data sources of all sites are listed in Table S5.

845
846



847
848
849

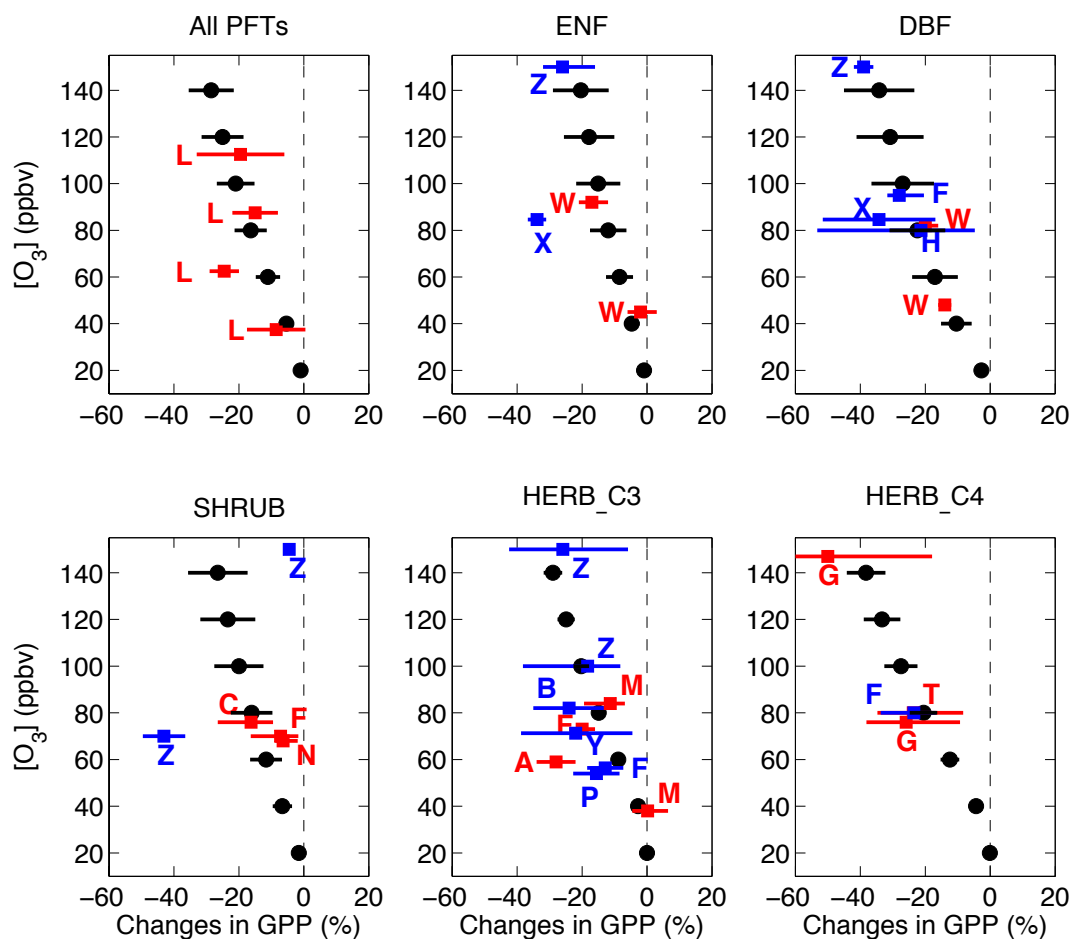


850
851
852
853
854
855
856
857
858
859

Figure 4. Evaluation of simulated radiation fluxes by ModelE2-YIBs. Panels show summertime surface (a) total shortwave radiation (units: W m^{-2}) and (d) diffuse-to-total fraction with (b, e) observations from 106 sites. Simulation results are from G10ALLNO3 performed with the climate model NASA ModelE2-YIBs (Table S2). The correlation coefficients (r), relative biases (b), and number of sites (n) for the comparisons are listed on the (c, f) scatter plots. The blue points in the scatter plots represent sites located within the box regions in southeastern China as shown in (a).



860

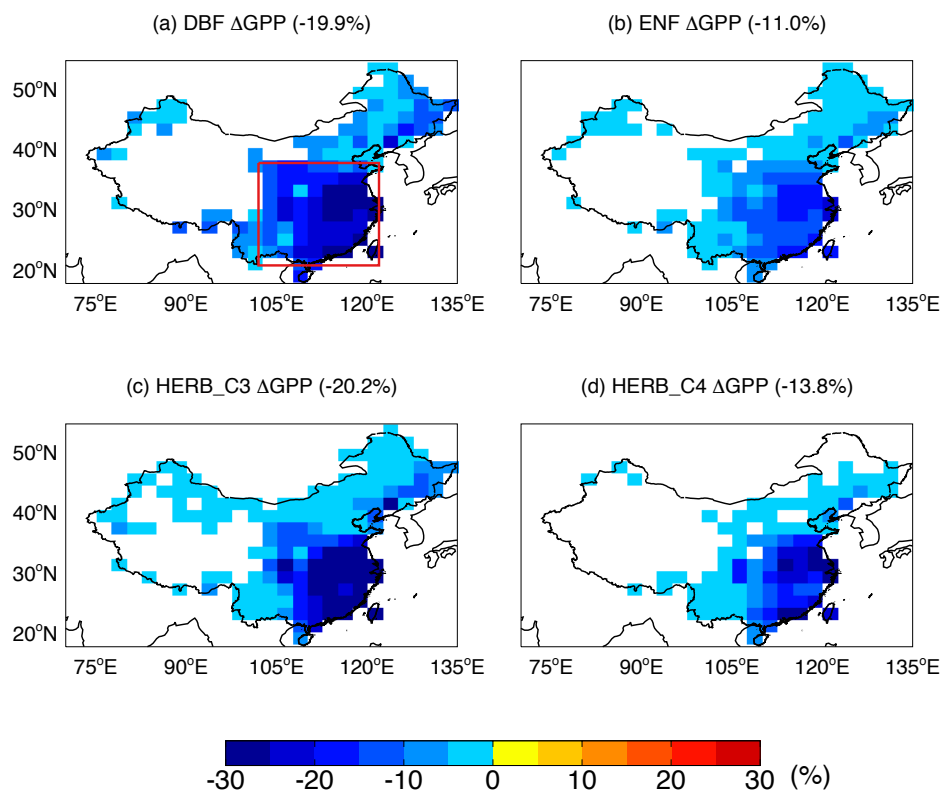


861
 862
 863
 864
 865
 866
 867
 868
 869
 870
 871
 872

Figure 5. Comparison of predicted changes in summer GPP by O_3 with measurements. Simulations are performed using the offline YIBs vegetation model (Table S3) and averaged for all grid squares over China weighted by the area of a specific PFT. Black points show the simulated mean reductions with error bars indicating damage range from low to high O_3 sensitivity. Solid squares with error bars show the results (mean plus uncertainty) based on measurements reported in the literature (Table S1). Experiments performed for vegetation types in China are denoted with blue symbols. The author initials are indicated for the corresponding studies.



873
 874



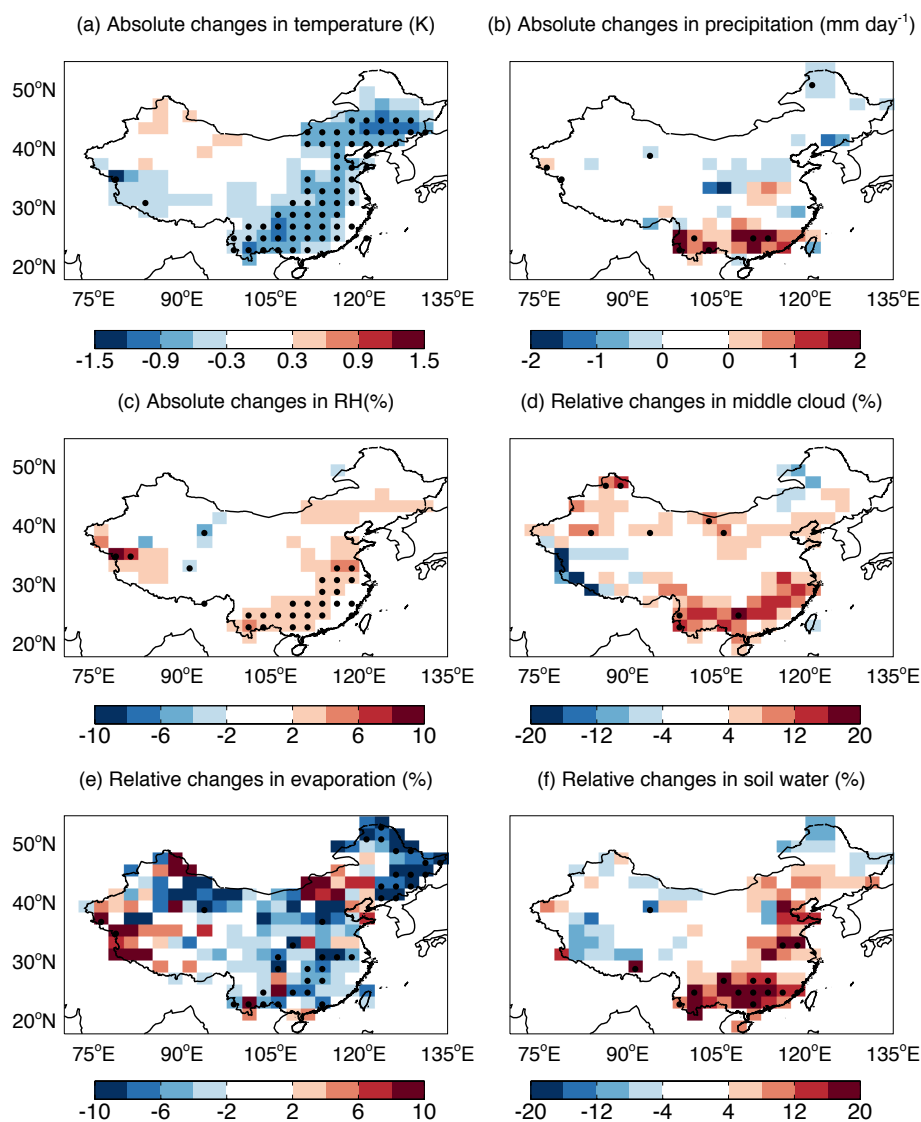
875
 876

877 **Figure 6.** Predicted offline percentage damage to summer GPP caused by O₃. Panels
 878 show the damages to (a) ENF (evergreen needleleaf forest), (b) DBF (deciduous
 879 broadleaf forest), (c) C3 herbs, and (d) C4 herbs over China in the year 2010. Simulations
 880 are performed with the climate model ModelE2-YIBs, which does not feed O₃ vegetation
 881 damages back to affect biometeorology, plant growth, and ecosystem physiology. The
 882 results are averaged for the low and high damaging sensitivities:

$$883 \quad \frac{1}{2}(\text{G10ALLHO3_OFF} + \text{G10ALLLO3_OFF}) / \text{G10ALLNO3} - 1) \times 100\%$$

884 The average value over the box domain of (a) is shown in the title bracket of each
 885 subpanel.

886
 887

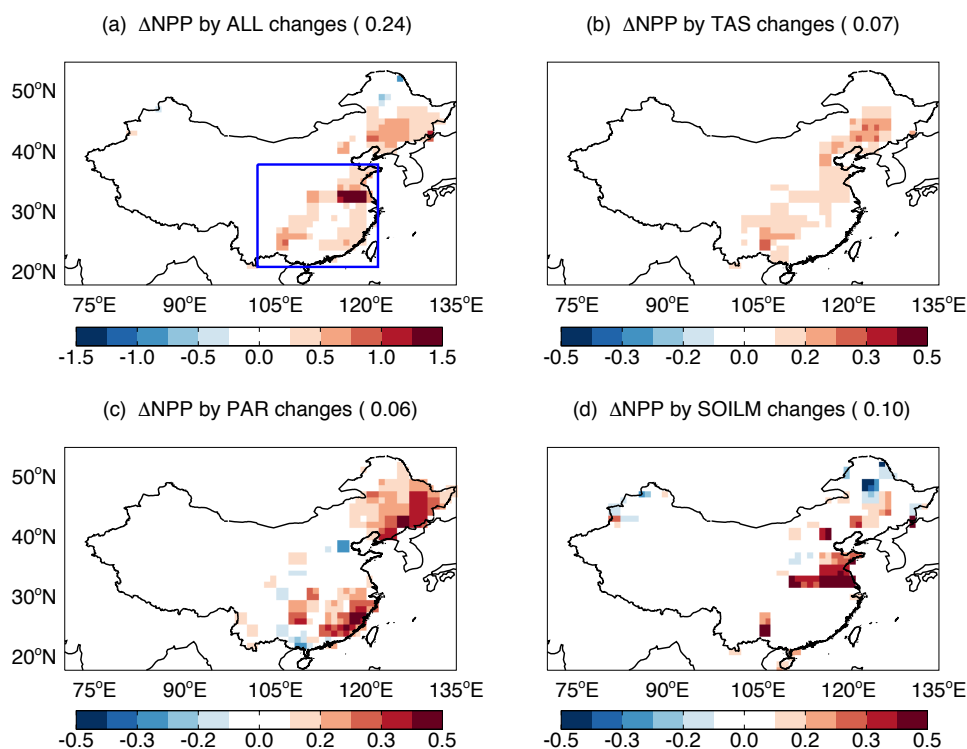


888
 889
 890
 891
 892
 893
 894
 895
 896
 897

Figure 7. Changes in summer meteorology due to direct radiative effects of anthropogenic aerosols. All changes are calculated as the differences between the simulations G10ALLNO3 and G10NATNO3. For (a) temperature, (b) precipitation, and (c) relative humidity, we show the absolute changes as G10ALLNO3 – G10NATNO3. For (d) middle cloud cover, (e) evaporation, and (f) soil water content, we show the relative changes as $(G10ALLNO3/G10NATNO3 - 1) \times 100\%$. Significant changes ($p < 0.05$) are marked with black dots.

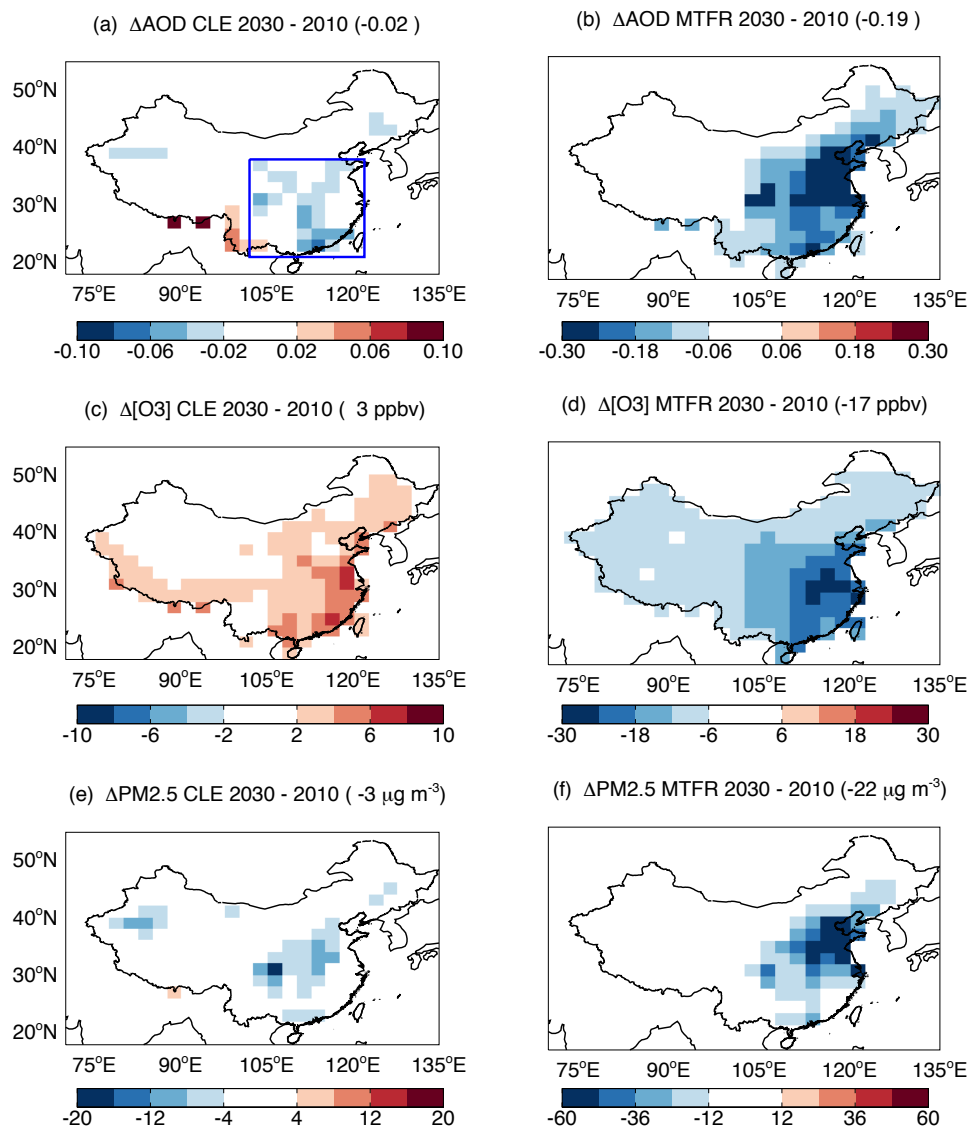


898
899
900



901
902
903
904
905
906
907
908
909
910
911
912

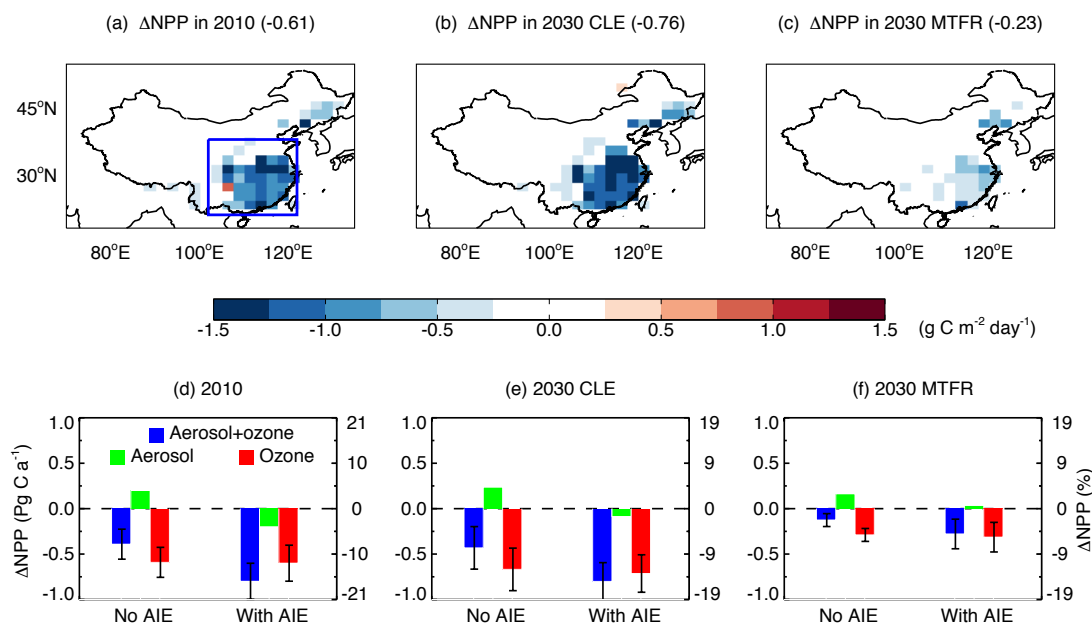
Figure 8. Decomposition of aerosol-induced changes in summer NPP. Changes in NPP are caused by aerosol-induced changes in (b) surface air temperature, (c) photosynthetically active radiation (PAR), (d) soil moisture, and (a) the combination of above three effects. Simulations are performed with the offline YIBs vegetation model driven with meteorological forcings simulated with the ModelE2-YIBs climate model (Table S4). The color scale for the first panel is different from the others. The average NPP perturbation over the box domain in a is shown in the bracket of each title. Units: $\text{g C m}^{-2} \text{ day}^{-1}$.



913
 914 **Figure 9.** Predicted changes in summertime air pollution by 2030. Panels shown are for
 915 (a, b) AOD, (c, d) $[\text{O}_3]$, and (e, f) $\text{PM}_{2.5}$ concentrations for the year 2030 relative to 2010
 916 based on scenarios of (left) current legislation emissions (CLE) and (right) maximum
 917 technically feasible reduction (MTFR). Results for the left panels are calculated as
 918 $(\text{G30ALLNO}_3 - \text{G10ALLNO}_3)$. Results for the right panels are calculated as
 919 $(\text{M30ALLNO}_3 - \text{G10ALLNO}_3)$. The average value over the box domain of (a) is shown
 920 in the title bracket of each subpanel.
 921



922
 923



924
 925

926 **Figure 10.** Impacts of air pollution on NPP in the whole of China. Results shown are
 927 combined effects of aerosol and O₃ on the summer NPP in (a) 2010, (b) 2030 with CLE
 928 scenario, and (c) 2030 with MTRF scenario. Results for the top panels do not include
 929 aerosol indirect effects (AIE) but do include the meteorological response to aerosol direct
 930 radiative effects. The average NPP perturbation over the box domain in (a) is shown in
 931 the bracket of each title. The perturbations to annual total NPP by aerosol, O₃, and their
 932 sum over the whole China are shown in (d-f) for different periods, with (right) and
 933 without (left) inclusion of AIE. Damages by O₃ are averaged for low and high
 934 sensitivities with error bars indicating ranges. The percentage changes are calculated
 935 based on NPP without AIE. Simulations are performed with the ModelE2-YIBs model.
 936 Only the significant changes ($p < 0.05$) are shown in (a-c).

937
 938